ENERGY

CONSERVATION

COO-2566-45

SODIUM-SULFUR BATTERY DEVELOPMENT PROGRAM, PHASE I

Progress Report, June 15, 1975—March 31, 1976

By
S. A. Weiner

July 1976

Work Performed Under Contract No. EY-76-C-02-2566

Scientific and Research Laboratory
Ford Motor Company
Dearborn, Michigan

U. S. DEPARTMENT OF ENERGY

Division of Energy Storage Systems

DISCLAIMER

NOTICE

COO-2566-45
Distribution Category UC-94c

FORD/ERDA SODIUM-SULFUR BATTERY DEVELOPMENT: PHASE I

Final Report

For Period June 15, 1975 - March 31, 1976

Submitted by

S. A. Weiner
Research Staff
Ford Motor Company
P. O. Box 2053
Dearborn, Michigan 48121

July, 1976

Prepared for:

THE U.S. ENERGY RESEARCH AND DEVELOPMENT ADMINISTRATION
UNDER CONTRACT NO. E (11-1) 2566

TABLE OF CONTENTS

LIST OF ILLUSTRATIONS

LIST OF ILLUSTRATIONS

ABSTRACT

This report was prepared in cooperation with staff members of the University of Utah and Aeronutronic Division, Ford Aerospace and Communications Corporation.

The pre-pilot facility for the batch production of β"-alumina tubing has been designed and remodeled. Critical items of capital equipment have been specified and placed on order. Work has begun on the construction of the pre-pilot spray dryer and the batch and continuous sintering furnaces. Preliminary contacts have been made with a commercial vendor of isostatic presses concerning the spray drying of materials suitable for automatic isostatic pressing. A tentative testing program has been arranged to permit evaluation of automatic isostatic pressing equipment for eventual purchase and installation in the pilot plant.

Two cells incorporating high power density electrode design and stainless steel containers for sodium and sulfur were designed, constructed and tested. The first cell delivered an average of 286 W/kg during one discharge cycle at 750 mA/cm^2. The energy density was 44 Wh/kg at this high current density whereas at 50 mA/cm^2 over 80 Wh/kg could be reached. The cell became non-faradaic after 45 days because of ceramic failure. The second cell has been put on test only recently. A cell with separate compartments for charging and discharging and with electrodes optimized for either task has been tested successfully.

Efforts to develop corrosion resistant sulfur container materials were inititated at Aeronutronic Ford. Static sodium tetrasulfide corrosion tests were conducted for 30 - 60 days at 400°C on substrates of pure chromium and iron, nickel, cobalt, aluminum, titanium, niobium, tantalum, zirconium, and molybdenum base alloys. These substrates were tested with and without various surface treatments and protective coatings.

The results showed that aluminum, molybdenum, ferritic stainless steels and Inconels, show varying degrees of promise, and further testing under dynamic conditions is recommended.

The first cell tested under this program was thoroughly examined after failure. The coating of graphite filled polyphenylene resin applied to the AISI 446 stainless steel container had not stood up satisfactorily perhaps owing to overheating. There were no signs of degradation of any of the seals.

SUMMARY

In the Electrolyte Development and Evaluation Task, which started on January 23, 1976, planning and preparation of the pre-pilot facility began.

Two cells with electrodes designed for high power output have been tested. The first cell delivered an average of 286 W/kg during one discharge cycle. It was tested to failure after 45 days. The second cell is identical in design to the first and initial test results are similar. This cell design aims at meeting the high power demands of vehicular applications.

A cell with individual electrodes optimized for charge and discharge in separate compartments was tested. The cell ran continuously for three months and was terminated without failure. From the technical point of view, this dual electrode concept deserves further exploration.

A number of materials and coating methods have been selected for use in the sulfur container based on the results of static corrosion tests. A dynamic test simulating battery conditions will be the final criterion before incorporation into prototype cells.

Detailed examination of the first high power cell after failure has revealed that the coating of graphite filled polyphenylene resin applied to the AISI-446 stainless steel had spalled partially, possibly as a result of overheating after ceramic failure.

INTRODUCTION

As a result of Ford Motor Company research on the sodium-sulfur battery, which began in 1960, the National Science Foundation (NSF) - Research For Applied National Needs (RANN) awarded contract NSF-C 805 to Ford, for the period July, 1973 to June, 1977. The program objective was to demonstrate the technical feasibility of the sodium-sulfur battery.

Because of the successes of the NSF-RANN program, ERDA granted, concurrently with the NSF-RANN Contract, a new 5 year program (Contract No. E (11-1) - 2566) in June of 1975, to design and develop a 35 kW battery for electric vehicle (EV) application and a 1 MW battery for electric utility load leveling (LL).

This report represents the work performed under this contract in the first year - Phase I. The tasks included (1) electrolyte development and evaluation; (2) electrode and cell development; (3) material development; and (4) cell life evaluation.

Task 1. Economic Evaluation and Determination of Material Availability

Work began on this task at the end of the third quarter.

Task 2. Electrolyte Development and Evaluation (Pre-Pilot)

Most of the work in Phase I beginning January 23, 1976, has been devoted to the renovation and preparation of space (∿ 1200 square feet) for the pre-pilot production facility which will be used in Phases II and III to supply sealed units of β"-alumina tubing. This renovation and remodeling has been completed. A schematic diagram for the lay-out of the pre-pilot facility is presented in Figure 2.1.

Critical items of equipment for the pre-pilot facility such as the isostatic press and compressor, the twin shell blender, and components for the spray dryer, the various bisquing, sintering, and annealing furnaces, and the electrical conductivity apparatus have been specified and placed on order.

Work has begun on the design and construction of the pre-pilot spray dryer and the sintering furnaces (batch and continuous pass-through).

The transfer of the current seal technology from Ford to the University of Utah began March 29, 1976.

Preliminary contacts have been made with Pentronix, Inc., concerning the spray drying of materials suitable for automatic isostatic pressing. A tentative testing plan has been arranged to allow us to evaluate automatic isostatic pressing equipment for eventual purchase and installation in the pilot plant.

Task 3. Electrode and Cell Development

(a) High Power Electrode

To meet electrically the high power requirements for acceleration of passenger cars, it is necessary to develop cells which provide high power

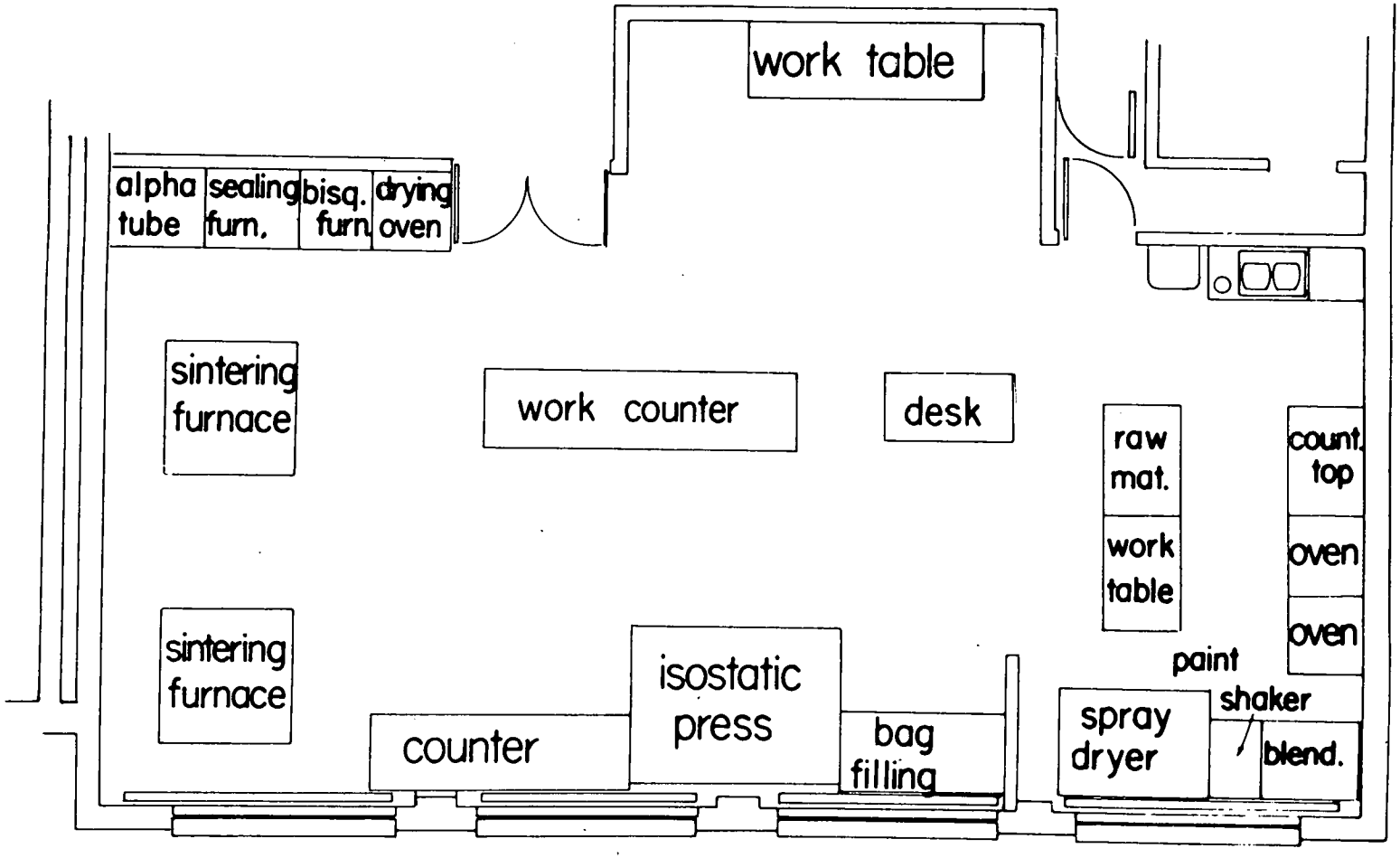

Figure 2.1 Layout of Pre-Pilot Facility

capability with moderate energy storage. The design of such cells can be based on the use of thin graphite felt electrode structures surrounding a tubular conducting ceramic. The purpose of this task is to design and then measure the performance of such cells. The thickness and compression of the graphite felt which yields the most satisfactory match of cell performance to electric vehicle needs will be selected.

Two cells incorporating high power density electrode design and stainless steel reservoirs for the sodium and sulfur compartments were designed, constructed, and evaluated. The components and assembled cell are shown in Figures 3.1 and 3.2. The sulfur electrode consists of graphite felt compressed to about twice density and inserted into the 3 mm gap surrounding the 1 cm diameter β"-alumina tube (9.0, 0.8, 90.2 wt % Na_2O, Li_2O, Al_2O_3). The felt was bonded to the depassivated inside surface of AISI 446 stainless steel tubing by a film of graphite filled polyphenylene resin.

Several procedures were necessary to seal the cell. The stainless steel reservoir for sodium was brazed to the nickel member of a brazed nickel-alpha alumina subassembly. The alpha alumina member of the subassembly was butt sealed to a 4.5 cm long alpha alumina tube by a borosilicate glass. The seal for the sulfur container involved a glass seal between the flared end of the metal tube and an α - alumina washer, and between the washer and the α - alumina tube.

The end caps and fill spouts were welded to the reservoirs following the filling operation, the fill spouts were sealed by a pinch off operation.

In cell ERDA-1 20 grams of sulfur and 20 grams of sodium were inserted so that the cell would operate sulfur limited. The theoretical capacity based on the amount of sulfur was 11.1 Ah. Total cell weight was 137 grams yielding a theoretical energy density of 162 Wh/kg. Following an initial discharge of 11.6 Ah, the cycle capacity was 5.9 $\pm$ 0.1 Ah under conditions of $J_c = J_d = 50$ mA/cm^2, 300°C, and voltage limits of 2.5 and 1.5 V.

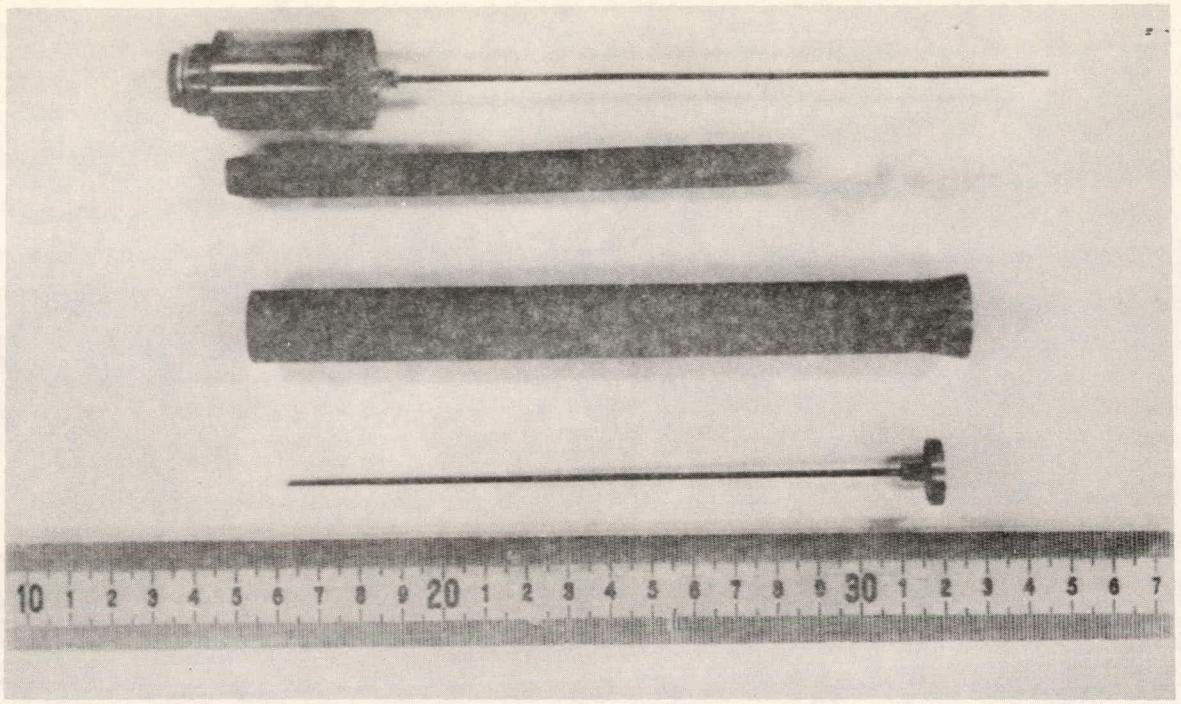

Figure 3.1 Components For High Power Density NaS Cell

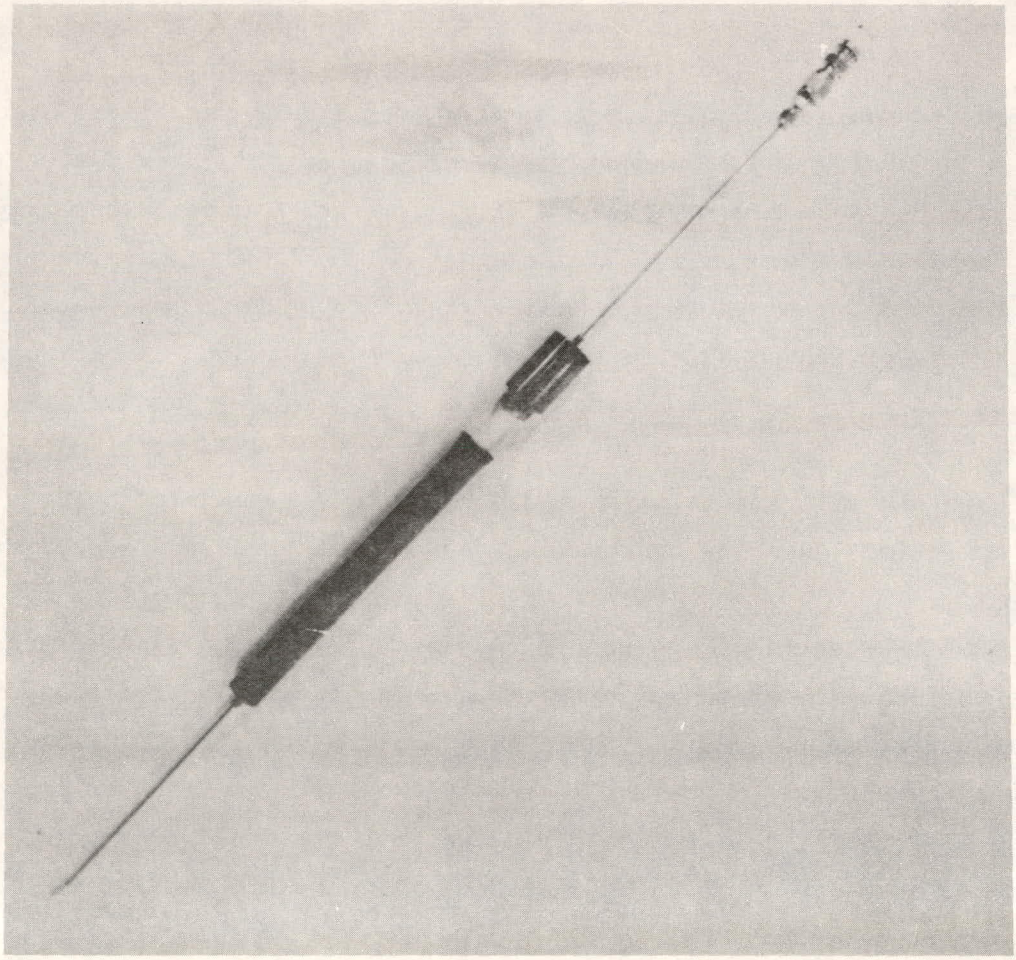

Figure 3.2 Assembled Cell

Cell operation under these conditions is limited to the one phase region of the Na-S phase diagram, i.e. Na_2S_3 - Na_2S_5. This limited capacity is not considered a disadvantage for the high power density cell because we believe that operation in the one phase region is necessary to provide low cell resistance for pulsed loads arising during vehicular operation.

Cell characteristics were obtained for different charge and discharge rates at 300°C and are shown in Figure 3.3. Discharge at high rates confirmed the power delivery capabilities projected from low current cycling operation. At 750 mA/cm^2 (33.75 A), the cell delivered 41.4 W (302 W/kg) for a short time, and 39.2 W (286 W/kg) averaged over the discharge cycle. At 750 mA/cm^2, the cell delivered over 6 Wh (44 Wh/kg), whereas at 50 mA/cm^2, the energy density was over 80 Wh/kg. The measured power density and energy density for ERDA-1 obtained at various discharge current densities are given in Figure 3.4.

Following two weeks of cycling at current densities $J_c = J_d = 50$ mA/cm^2 and measurement of the charge/discharge characteristics, the cell capacity had dropped to 4.6 Ah from the initial 5.9 Ah. Cell operation now was entirely limited to the one phase region of the Na-S phase diagram. The charge and discharge rates were then increased to more realistic values of $J_c = 100$, $J_d = 200$ mA/cm^2. The cycle capacity was 3.2 Ah, and remained unchanged for 18 days and 400 cycles, before slight non-faradaic behavior was observed and the cell failed after 45 days of operation.

After failure, the cell was examined and found to have a cracked β"-ceramic throughout the middle portion of its length. This finding explains the non-faradaic behavior prior to failure, and the apparent cell open circuit condition at its termination, since polysulfide had formed within the tube and had broken contact of the sodium to the β"-alumina. The α-β"-alumina seal area and the upper portion of the tube appeared unattacked, but the lower section of the tube, though intact, appeared to be highly stressed.

Some changes were observed in the nature of the polyphenylene coating which was used to protect the AISI 446 steel. Shiny deposits had formed within the layers, and the inner surface of the polyphenylene appeared to have been altered.

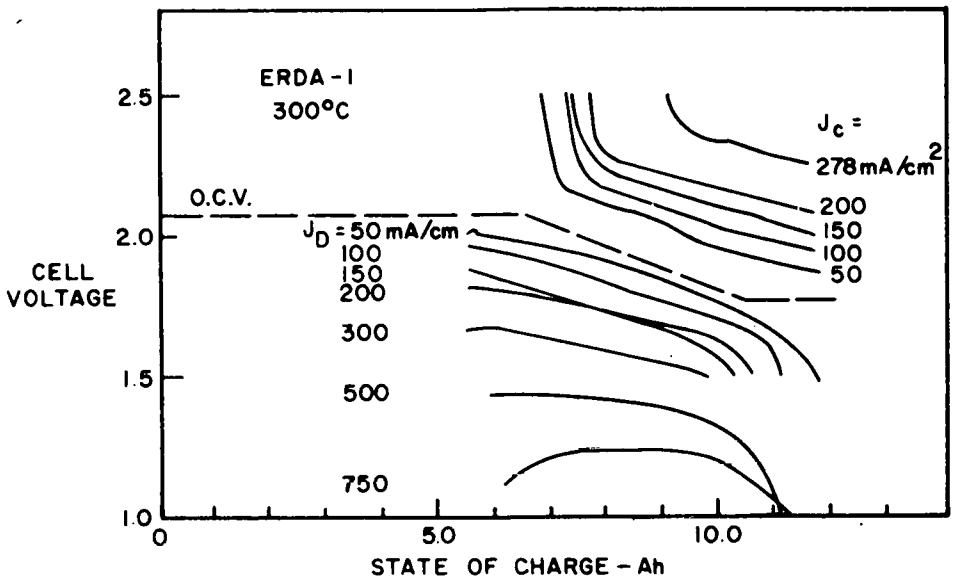

Figure 3.3 Charge/Discharge Characteristics of Cell

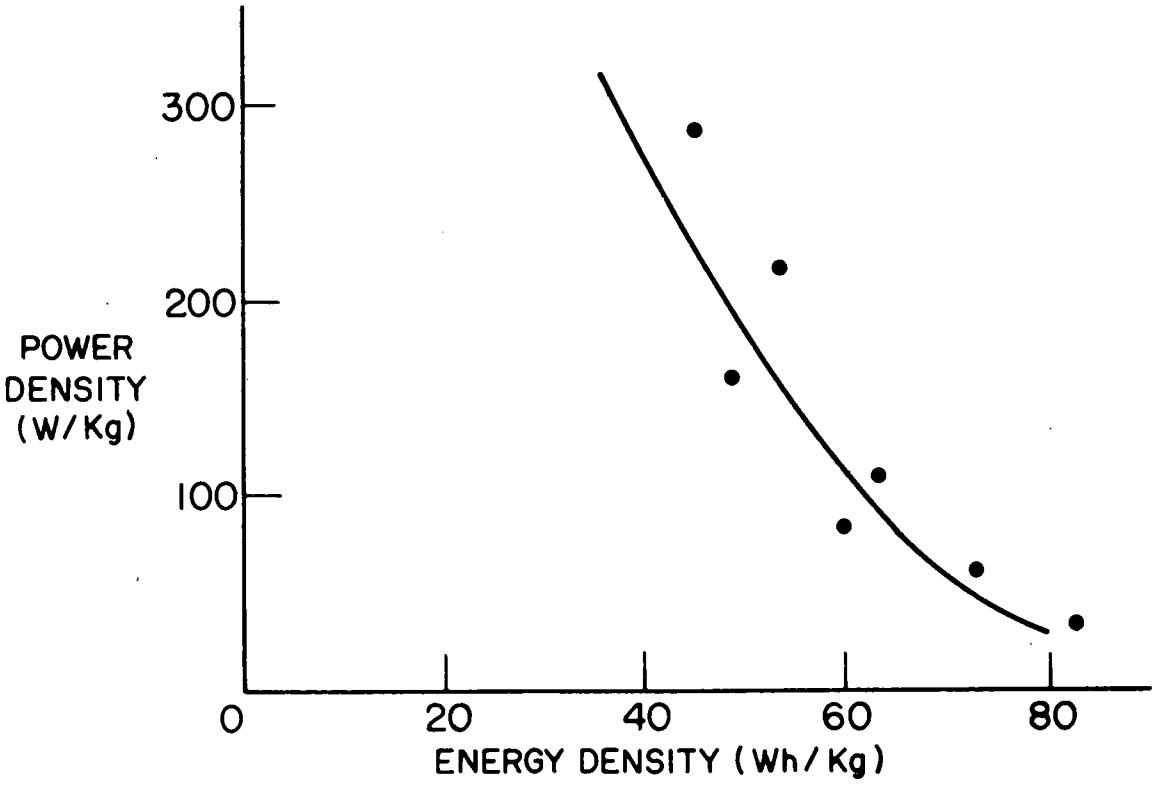

Figure 3.4 Power Density vs. Energy Density

The second cell is identical to the first, except that it has been filled with 22 grams of sulfur to give it a theoretical capacity of 12.3 Ah. The cell was recently put on test. Initial results indicate slightly larger cycle capacity and slightly higher cell resistance for ERDA-2 than for ERDA-1. Following a brief characterization of performance at 300°C, the cell will be tested more thoroughly at 350°C.

(b) Improved Charge Efficiency in High Energy Cells

For load leveling applications, high charge voltage efficiency is especially important. The performance of the graphite sulfur electrode is limited on charge because the non-conductive sulfur covers the graphite surface as the electrode is charged into the two phase sulfur plus polysulfide region. Numerous methods have been proposed to overcome this problem [1,2] but they need further development.

One such method is the use of metal electrodes. Metal electrodes do not become blocked by sulfur because they are preferentially wetted by polysulfide rather than sulfur, whereas the opposite is true for graphite. The wetting criteria may be generalized as: polysulfide wettable materials are those whose surfaces are polar or have d-orbitals available for bonding. Certain metals, metal oxides and metal sulfides are included in this category.

Data were obtained previously [2,3] on a cell built in accordance with the schematic shown in Figure 3.5. A perforated stainless sheet with 40% open area surrounded the β"-alumina tube and served as the sulfur electrode.

The data at 330°C showed excellent rechargeability, yielding 96% of the theoretical capacity over a wide range of current densities. The cell performance was limited by the discharge. Interrupter measurements confirmed that the charging voltage could be accounted for by ohmic drop. Concentration polarization was zero. The flat charging curves indicated that polysulfide metal continues to be wicked between the metal and β"-alumina tube even as the cell filled with sulfur. By contrast, the best graphite electrode cells at similar temperatures show higher charging voltages with the voltage continuously increasing during charge due to concentration polarization and ohmic drop. Unfortunately, the stainless steel as well as most other metals are corroded appreciably by sodium polysulfide.

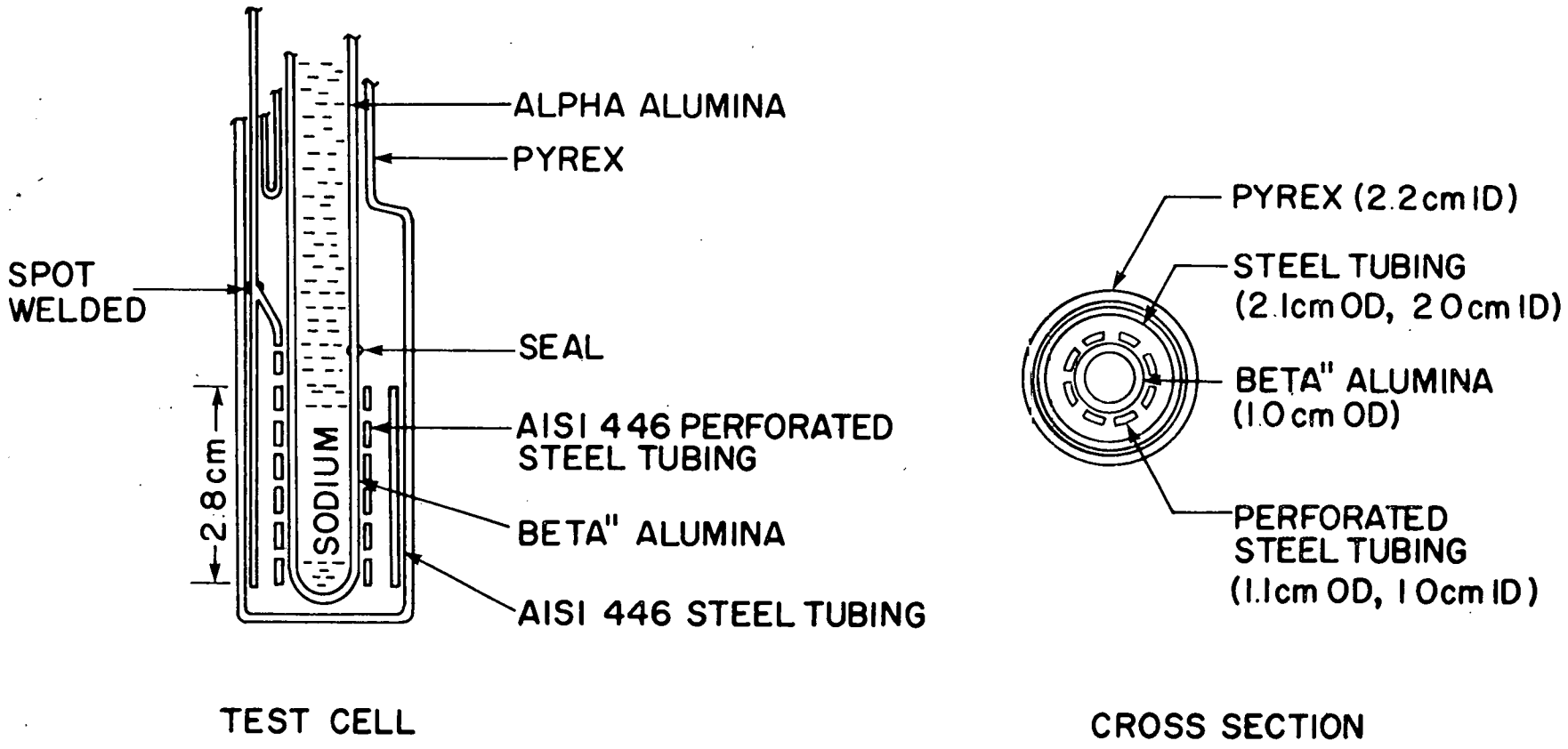

Figure 3.5 Schematic of Metal Electrode Cell

It has been shown previously that stainless steel can be anodically protected from corrosion by polysulfides [3,4]. These observations led to the design of a durability test of a metal electrode which is maintained under anodic protection. The cell incorporates a separate graphite electrode for discharge and a metal electrode for charge. The dual electrode cell is shown schematically in Figure 3.6. During charge the lighter sulfur formed at the perforated metal electrode should rise to the top. During discharge the polysulfide produced at the graphite electrode should sink to the bottom. Transport of the reaction products between the electrodes is expected to occur by free convection.

Rather than cycling the cell, as one would do in actual use, the graphite electrode was discharged continuously and the metal electrode was charged continuously. This was done at a melt composition such that the upper half of the cell should be filled with sulfur and the lower half with sulfur saturated polysulfide. In this way, corrosion data under constant conditions could be obtained.

Cell operation was begun by discharging at the graphite electrode while a slight positive charge was maintained on the metal electrode to provide anodic protection as the heavier polysulfide began to fill the bottom of the cell. A probe microelectrode, positioned midway between the upper and lower electrodes, sensed the resistance of the melt between the probe and sodium column. The resistance changed abruptly when the sulfur/polysulfide interface passed by the probe electrode, as shown in Figure 3.7. The net ampere-hours discharged in the cell at the time of the abrupt resistance charge coincided with the value calculated for the interface to pass the probe electrode on the assumption that the two phases separate completely into sulfur and $Na_2S_{5.2}$.

After a slight additional discharge, cell operation was adjusted so that the charge and discharge currents were equal. Under this condition no change in melt composition should occur during the extended duration of the test.

After 2069 hours of continuous operation the cell was recharged by operating at higher charge than discharge current, so that the interface level again

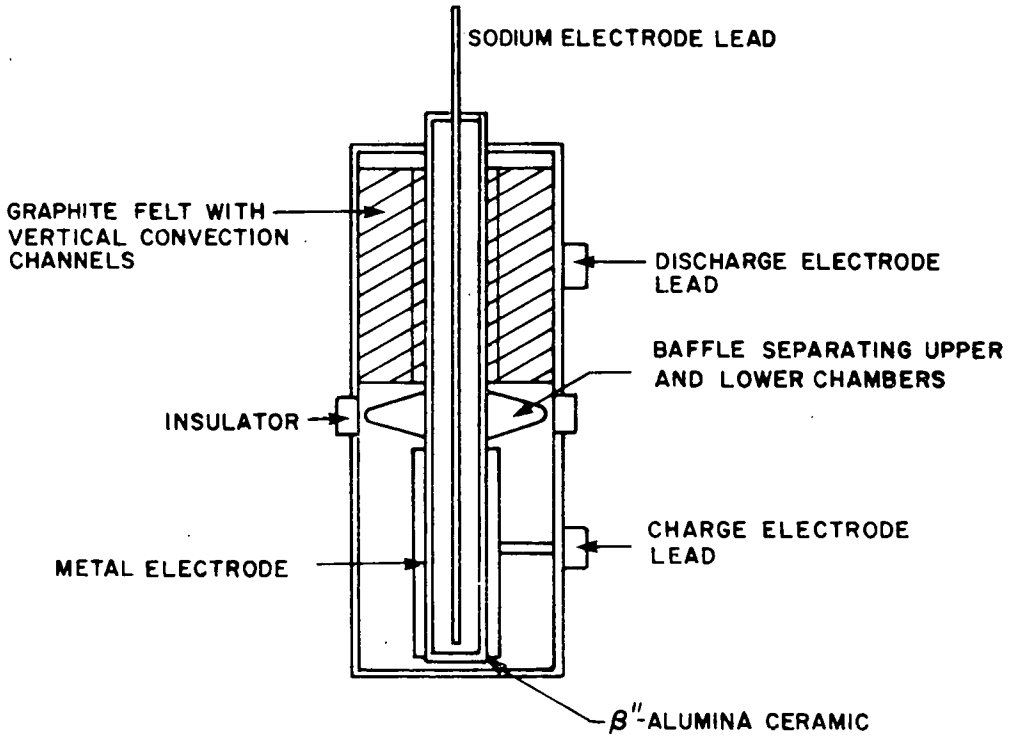

Figure 3.6 Schematic of Dual Electrode Cell

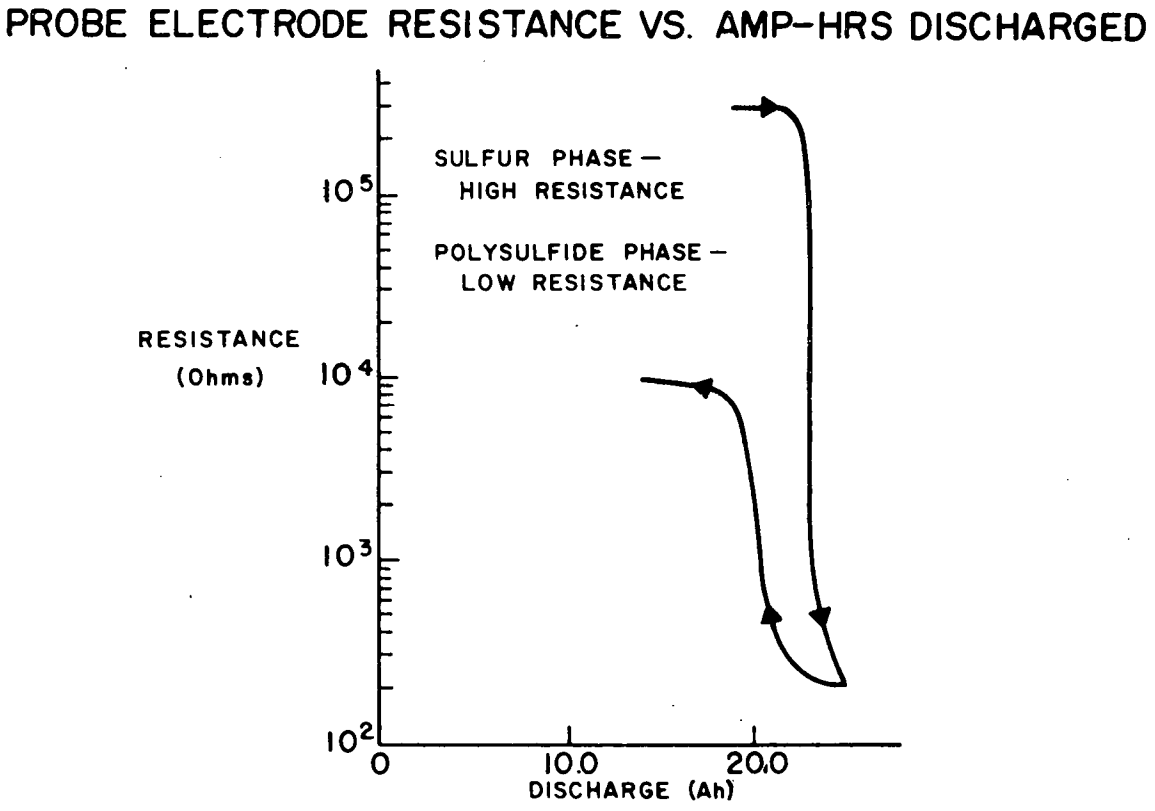

Figure 3.7 Resistance of Probe Electrode

passed the probe electrode. The probe to sodium resistance is shown in Figure 3.7. The slower change suggests that phase separation was not as distinct as at the beginning of cell operation. This suggests that either some emulsification of the phases occurred or that a column of polysulfide continued to contact the probe electrode as the interface level fell below the probe tip.

The performance of the dual electrode cell, with the graphite electrode on continuous discharge and the metal electrode on continuous charge, is summarized in Figure 3.8.

Ceramic resistance and electrode lead resistance have been subtracted from the charge and discharge potential drops. The voltage efficiency of both electrodes was excellent at first, and then began to deteriorate. Interrupter measurements revealed that a concentration polarization was building up at the metal electrode, in contrast to the zero concentration polarization in the previous metal cell with the flat charging curves. The graphite discharging electrode performance also decreased with time; most of the decrease was caused by an increase in iR drop. The cell was put through one charge/discharge cycle after 1700 hours of operation by adjusting the relative charge and discharge currents. Upon resumption of the initial operating conditions, the graphite electrode showed little change in performance; however, a short lived improvement was observed at the metal electrode.

After three months of continuous operation at 325^{o}C the test was terminated deliberately. The total charge transported during this period corresponds to 311 Ah/cm^{2} of ceramic covered by the perforated metal electrode. Examination of the cell showed that only 0.002 cm of the metal had corroded; whereas, when the stainless steel electrode of the previous cell was operated in a cycle mode and not continuously anodically protected, the corrosion rate was 200x greater. Thus, by means of anodic protection the physical structure of the electrode could be maintained during the desired life-time of the battery.

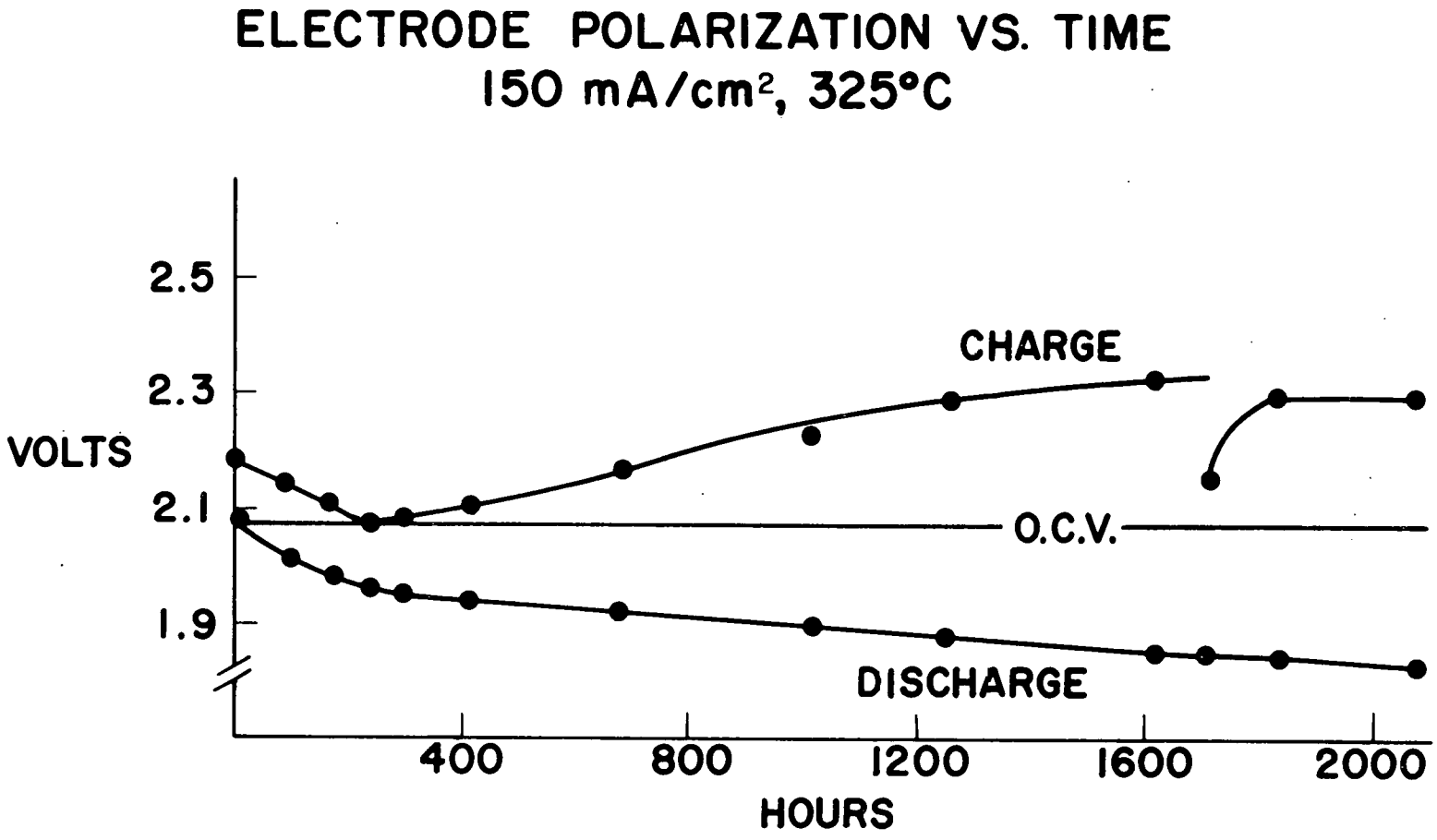

Figure 3.8 Electrode Polarization vs. Time

However, the effect of the corrosion products must be considered. Will they damage the β"-alumina ceramic? They did not do this during the time of operation of either the metal cell or the dual electrode cell. Will the corrosion products affect cell performance? In the previous metal cell, which was cycled, the corrosion products were dispersed throughout the cell, and had a minimal effect on electrode performance. In the dual electrode cell, in which the electrode was held at a continuous, high charging current, the corrosion products were found concentrated between the β"-alumina tube and the metal electrode. Apparently the slow buildup of concentration polarization is linked to the accumulation of corrosion products and the maintenance of high charging current. Indeed, when a low charging current is maintained for just one cycle, the polarization is reduced sharply, as can be seen, at 1700 hours, in Figure 3.8.

At the end of the 2069 hour cell test the upper graphite electrode was disconnected and the electrode polarization at the metal electrode was measured during continued charging. The polarization is plotted in Figure 3.9 in terms of the percent conversion of the sulfur-saturated sodium polysulfide in the cell to sulfur. A drastic increase in both iR drop and concentration polarization is observed.

This increase undoubtedly is related to the accumulation of corrosion products on the β"-alumina tube as polysulfide converts to sulfur and the dissolved corrosion products precipitate near the electrode.

In summary, we have learned from the dual electrode cell that:

1. Anodic protection of stainless steel can result in adequate lifetimes of the physical structure.

2. Free convection due to phase separation was sufficiently rapid to maintain cell operation at high rates for this metal and graphite electrode configuration.

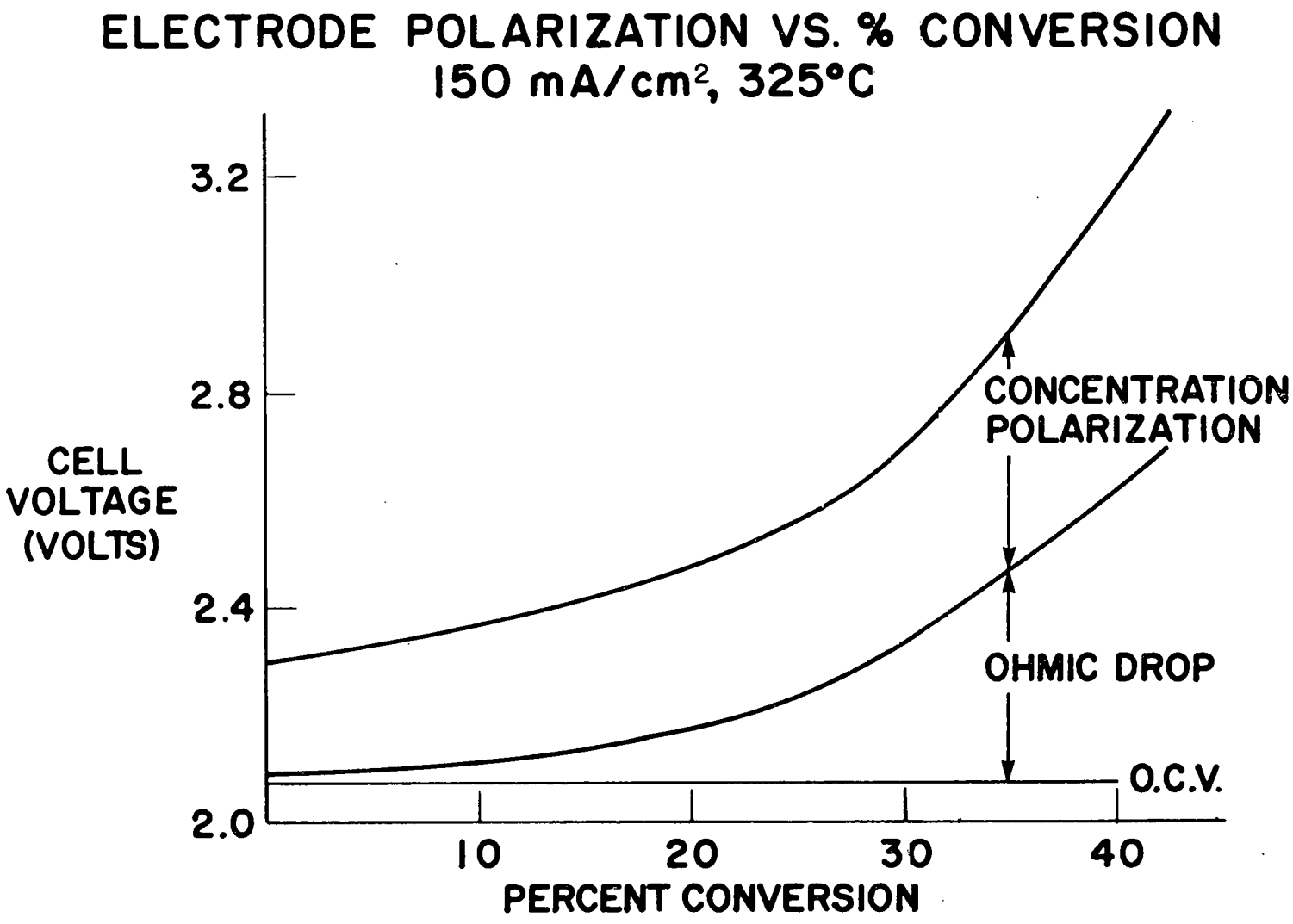

Figure 3.9 Electrode Polarization vs. % Conversion

3. Further work using stainless steel and other electrode materials preferentially wetted by polysulfide is required to explore if polarization due to corrosion products can be kept low.

Task 4. Materials Development

Development of a low-cost, highly reliable sulfur container is one of the more challenging aspects of cell development. Previous work [1,2,4] has shown that sodium polysulfide is highly reactive with most metallic materials at temperatures of 300 - 400°C, although metal oxides, graphite, carbon, and some resins appear to be stable. With this background information, a program consisting initially of static corrosion tests in sodium tetrasulfide was conducted on a matrix of various substrate materials with and without selected protective coating systems and/or surface treatments.

A rather broad spectrum of metals and alloys was selected, primarily those that are known to be corrosion resistant due to an inherent oxide layer or that can be passivated by a conversion coating. In addition, low cost was an important consideration in selection of some candidate materials. Armco iron, low expansion iron-nickel alloys, ferritic stainless steel, nickel base Hastelloys and Inconels, a cobalt base superalloy, aluminum, titanium, refractory alloys (Nb, Ta, Zr, and Mo base), and pure chromium were tested. Surface treatments and coating systems known to be amenable to high production rate processing were investigated on selected substrates.

Samples representing the various combinations of substrates, surface treatments, and coatings were evaluated after testing in static sodium tetrasulfide for 30 and 60 day periods. Although considerably more corrosion testing including thermal cycling, dynamic current tests and actual cell tests are required, the results of this initial screening evaluation are significant and indicate possible directions for further development.

(a) Approach

Test samples were cut from commercially supplied sheet stock. The specimens were 1" long by 1/2" wide; the thickness varied from 0.040" to 0.150".

Untreated metals and alloys were cleaned in detergent and tested as sheared. The edges and corners of the substrate alloys were machined round and ball milled to minimize edge effects on the coatings. These specimens then were given the various surface treatments and coatings. Most of the coatings and treatments were applied in commercial shops by established methods. The samples were inspected carefully, measured and weighed before testing.

The samples were loaded individually into a 16mm diameter by 120mm long pyrex tube, which had been necked down on one end and joined to a 6mm diameter evacuation tube. The large end of the 16mm tube was sealed off, encapsulating the specimen. The capsules were evacuated to less than 0.1mm Hg and passed into a glove box containing a dry argon atmosphere. Approximately 5 grams of Na_2S_4 was introduced into the capsule through the 6mm tube. This was enough chemical to immerse approximately one half of the specimen in the melt so that both liquid and vapor phase effects could be observed. The 6mm fill tube was swabbed clean, and a vacuum hose attached. The capsule was evacuated to less than 0.2mm of Hg and sealed off with a torch. A glass hook was formed on the sealed tube stub, and an Inconel wire ring attached. The specimens were lowered into individual holes in an aluminum block maintained at $400^{\circ} \pm 5^{\circ}C$ for the test period.

The Na_2S_4 was synthesized at Ford from high purity Na_2S and high purity sulfur.[2] Throughout the filling and sealing procedure, and while in storage, the Na_2S_4 was not exposed to the open atmosphere.

The untreated metals and alloys were tested for 60 days, and the surface treated and coated samples were tested for 30 days. After the test period, the capsules were cooled to room temperature and broken open. The appearance of the sample and the melt were noted. The sample and melt were immersed in a beaker of warm water and the Na_2S_4 was dissolved. The solution was decanted off, noting any precipitates. The specimen and any residue or spalled coating on the container bottom were examined with a stereo microscope. The thickness of any reaction products remaining on the sample were measured and the appearance noted. Any loose reaction product on the metal specimens was then removed mechanically. The cleaned specimen was weighed and measured and the corrosion rates calculated.

(b) Results and Discussion

As expected the untreated metals and alloys reacted to varying degrees during the 60 day exposure to sodium tetrasulfide. The iron, iron-nickel, and iron-nickel-cobalt alloys were attacked most severely, producing a low density solid reaction product 10 to 20 times the volume of the original metal. (See Figure 4.1)

Chromium metal and all alloys containing over 15% chromium were partially protected by a dense crystalline reaction layer (Figure 4.2), with the corrosion depth generally limited to less than 2 mils over the 60 day test period. The volume of these reaction products was up to 10 times the volume of the displaced metals. These layers spalled on cool down from the test temperature, and had little adhesion at room temperature.

Molybdenum was protected very well by a thin layer of what appeared to be molybdenum disulfide. This coating was quite adherent after cool down and cleaning. Molybdenum as an alloying agent did not provide corrosion resistance as is evidenced by the Hastelloy B specimen.

Alloys of titanium, niobium, and tantalum were corroded heavily. Zirconium exhibited reasonably good corrosion resistance and was used as a control material. A specimen was put into test each time a different batch of Na_2S_4 was used. Seven thirty-day test samples had an average corrosion of 9.94 mg/cm^2 with an average deviation from the mean of 10.5%. 3003 aluminum alloy exhibited very good corrosion resistance in the as received condition.

Armco iron and iron-42% nickel were poor substrate materials as they reacted with the melt through any coating imperfections and shed the coatings. Two samples of AISI 446 and aluminum behaved similarly. It is surmised that the application of some coatings activates the substrate surface through removal of any natural passivation layers, thus accelerating corrosion.

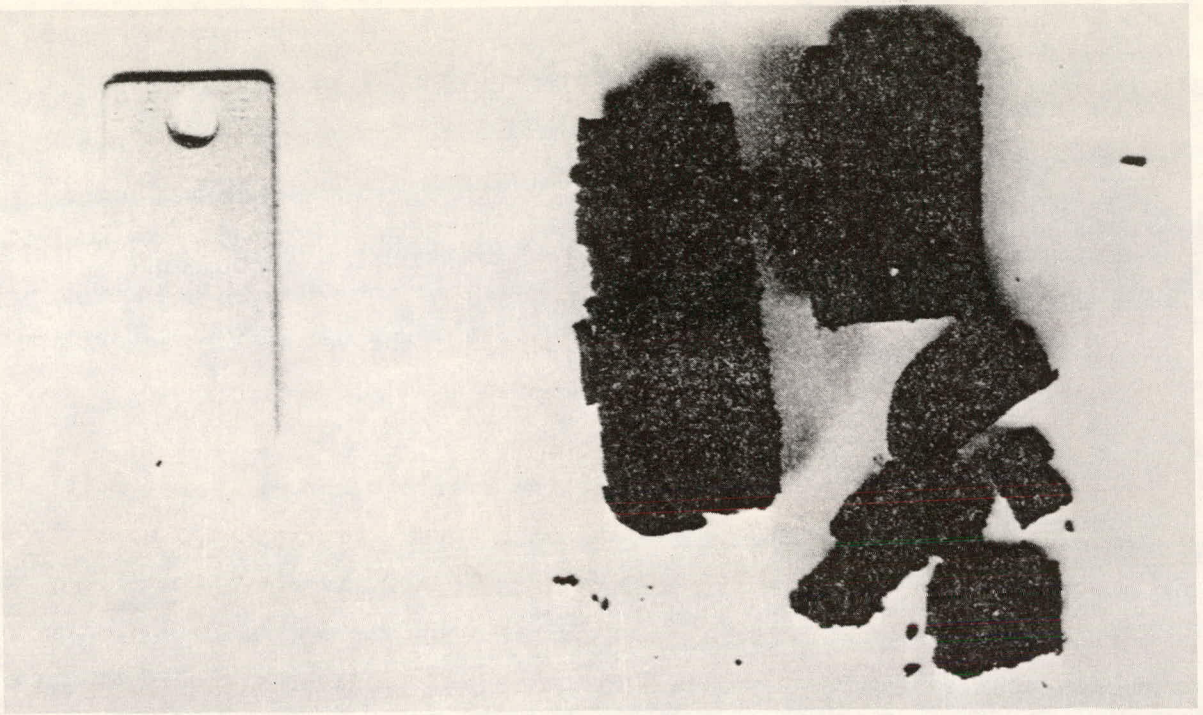

Figure 4.1 Massive Corrosion of Iron-Nickel Specimen

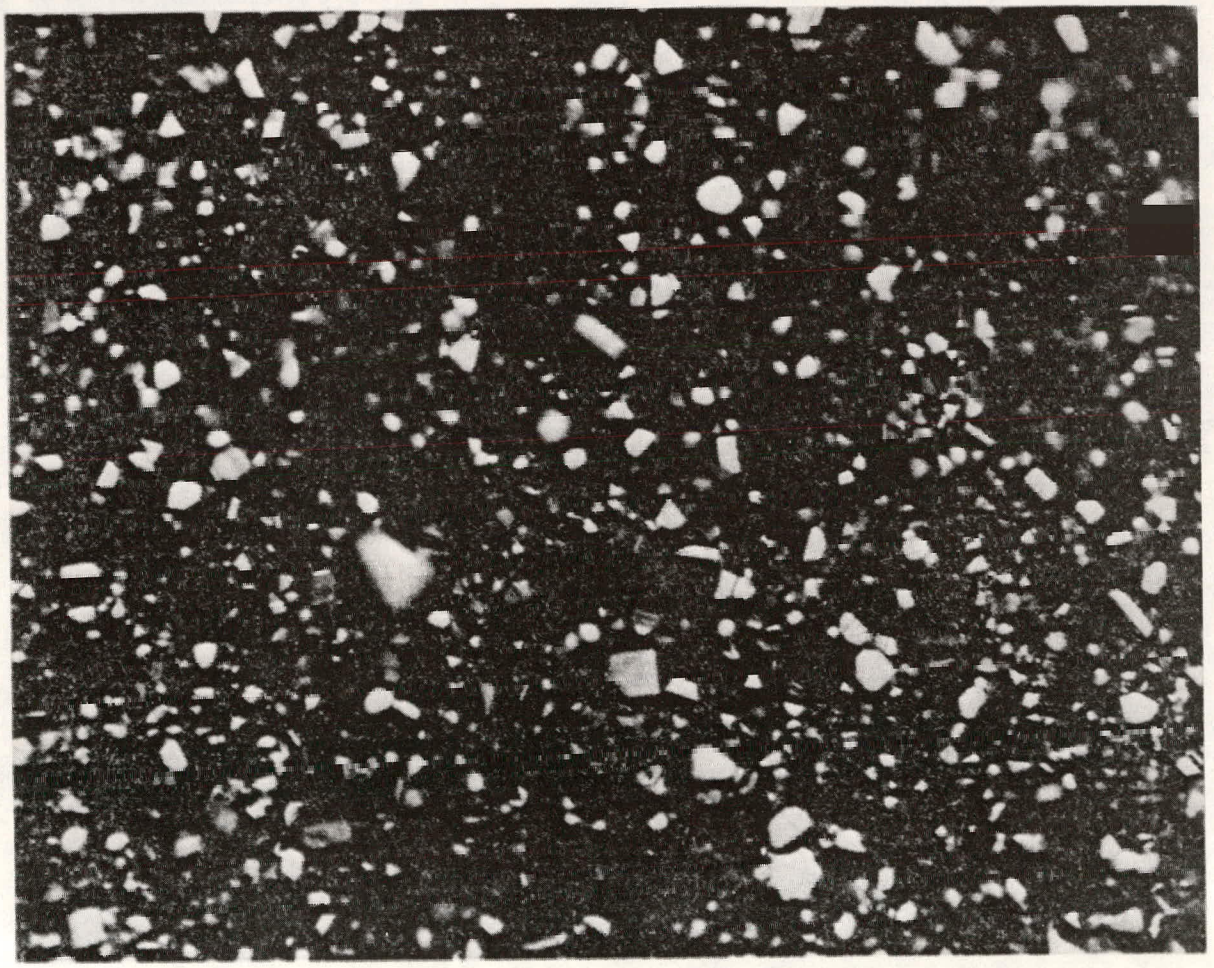

Figure 4.2 Crystalline Reaction Product on AISI-446

(c) Conclusions

Based on the initial static sodium polysulfide corrosion tests, the following materials appear worthy of further evaluation as substrates:

1. 3003 aluminum
2. Molybdenum
3. 400 series stainless steels
4. Inconels

The importance of testing these candidates under actual cell conditions is recognized and accordingly, containers are to be fabricated from selected materials and tested during the latter part of Phase I and during Phase II.

(d) Container Fabrication

Prototype containers 1-1/2" in diameter x 8" long have been fabricated using AISI 430 and 3003 aluminum as substrate materials. The coated containers were baked at 400°C in air for several hours and cooled to room temperature with no apparent degradation of the components.

The resistance was measured from the graphite current collector, to the outside of the containers. A 2" long copper tube was used as the inside probe, and a clamp as the outside probe. The resistance through one electrode leg was: 120 mΩ for the stainless steel container and 600 mΩ for the aluminum container. The particular graphite felt used had a resistivity of 0.06 Ω cm.

Task 5. Cell Life Evaluation

As of March 31, 1976, the only results available were obtained from a post-mortem analysis of high power cell ERDA-1.

At this stage in the post operative examination of components of the prototype cell (ERDA No. 1 - designed to optimize power density) it appears that the seals have performed adequately. Though the

protective coating on the sulfur container had degraded, that did not seem to be the principal cause of electrolyte degradation and cell termination.

(a) Non-destructive Evaluation

Upon cool down and removal from the furnace visual inspection of the exterior of the cell indicated no signs relating to cell malfunction. X-ray radiographs then were made in two mutually perpendicular directions. A sketch based on those radiographs, bearing on the distribution of cell contents, is shown in Figure 5.1. It was evident that the contents of the ceramic tube were no longer pure sodium and the space occupied by what was later found to be sodium polysulfide is shown shaded. Sodium appeared to fill the ceramic tube above the 4.5 cm position except for a partial void just under the upper seal: it was estimated that 9 to 10 grams of sodium remained in the upper portion of the cell.

The graphite felt was not distributed with complete uniformity along the length of the cell, as shown by light, fuzzy, transverse narrow bands in the radiography, starting about 3.6 cm below the top of the container and extending nearly to the bottom. Subsequent examination showed that these were gaps between the graphite felt rings, some of which had been filled with polysulfide.

(b) Cell component inspection (disassembly)

(i) Sodium reservoir

The sodium reservoir was separated from the cell by cutting the α-alumina tube at the partial void (indicated by radiography) beneath the α-alumina-metal container seal.

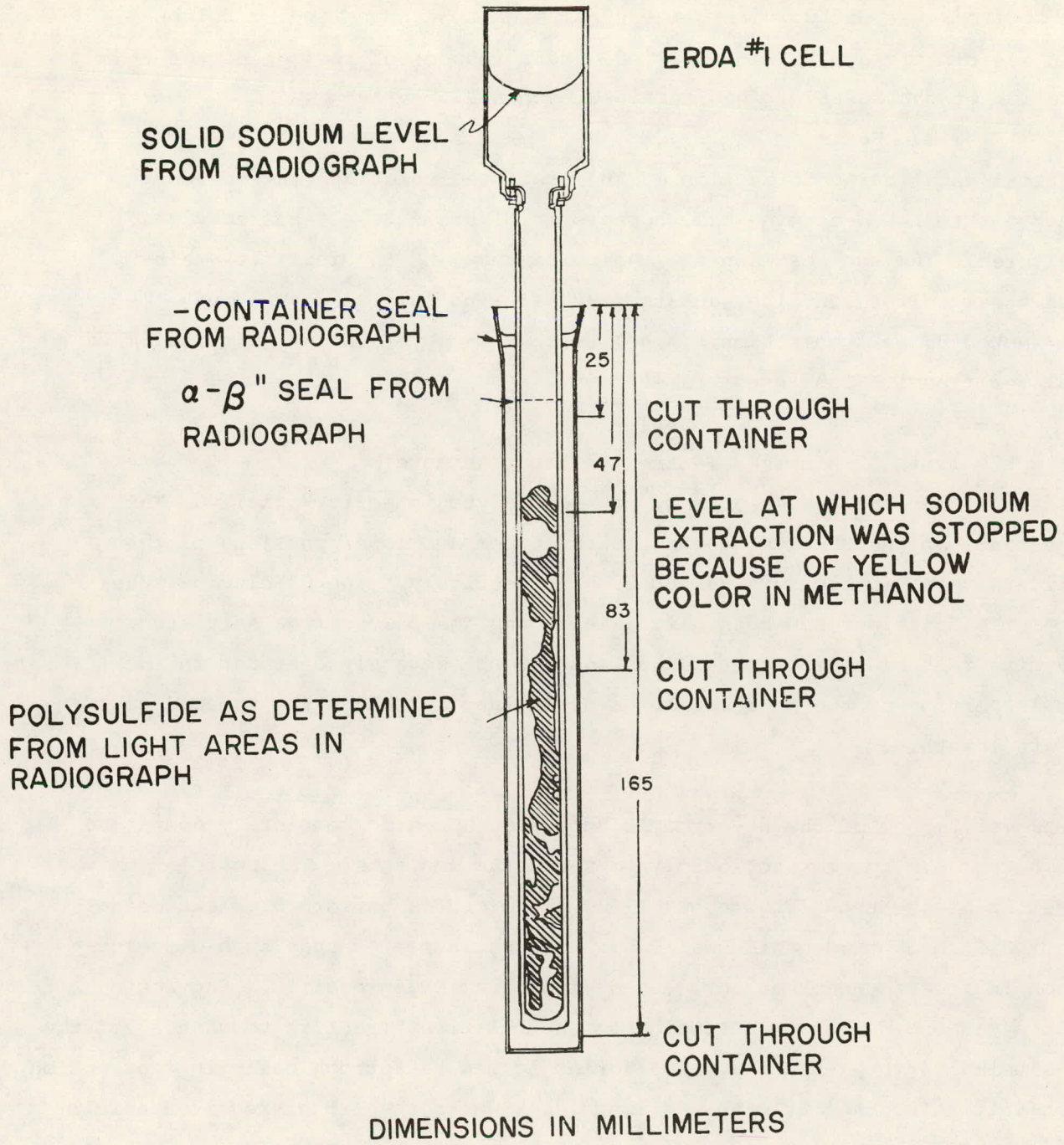

Figure 5.1 Schematic of Cell Indicating Disposition of Sodium Polysulfide from Radiographic Interpretation

From Figure 5.2 it is evident that sufficient sodium remains in the tube section at that location to provide an electrically conducting path from the sodium reservoir down into the β"-alumina tube. The sodium column then was dissolved with methanol and visual inspection indicated that the interior of the reservoir had remained unchanged.

(ii) Seals

An axial metallographic section of the seal used to attach the sodium reservoir to the α-alumina tube appears in Figure 5.3. It has remained unaltered. The seal between the α-alumina tube and the ferritic stainless steel sulfur container and the α-β"-alumina join also appeared uneffected by cell operation. A helium leak check of the α-β-alumina seal verified its continued hermeticity.

(iii) β"-Alumina electrolyte (and contents)

Visual inspection reveals a range of electrolyte integrity axially. The appearance of the β"-alumina tube in the upper and lower portions of the cell are shown in Figure 5.4a and 5.4b respectively. The β"-alumina tube, after the container had been slit axially and the polysulfide saturated graphite felt had been removed, was found to be severely degraded in the middle portion of the cell but to have remained intact in the upper 2 cm of its length.

The lower 2.5 cm of the β"-cermamic tube also appeared completely sound and the bottom 1.2 cm was sectioned to observe the contents. The bottom exterior of the tube (Figure 5.4c) was discolored a uniform gray extending about 0.5 cm up the outside wall. Experience indicates that such discoloration in itself cannot be correlated with ceramic degradation. Sectioning with a diamond disk drew attention to the relative "fracture toughness" of the β"-alumina versus α-alumina. The former failed catastrophically in crossection upon initiating the cut with a diamond disk while the latter required a full through cut.

The bottom of the ceramic tube section in Figure 5.4a, corresponding to a position 8.3 cm from the top of the container (see Figure 5.1), is filled only partially with reactant, confirming the radiographic evidence. The composition of the contents in the β"-alumina tube at this location was found to be 46.1% Na and 53.2% S by weight. Visual inspection, revealing alternate layers of light and dark constituents

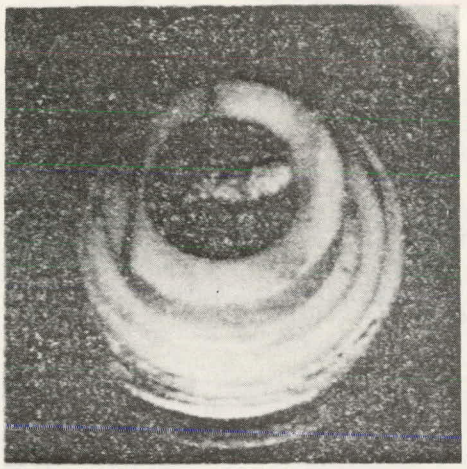

Fig. 5.2 Section of α-Al_2O_3 Tube, partially filled with Sodium, Illustrating Unaffected Condition

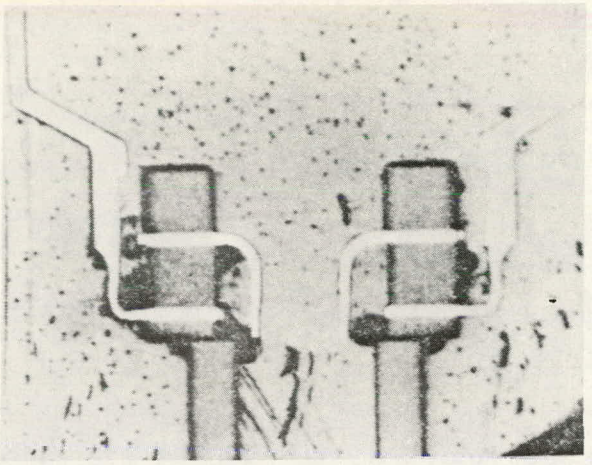

Fig. 5.3 Axial Metallographic Section of α-Al_2O_3 to Sodium Container Seal

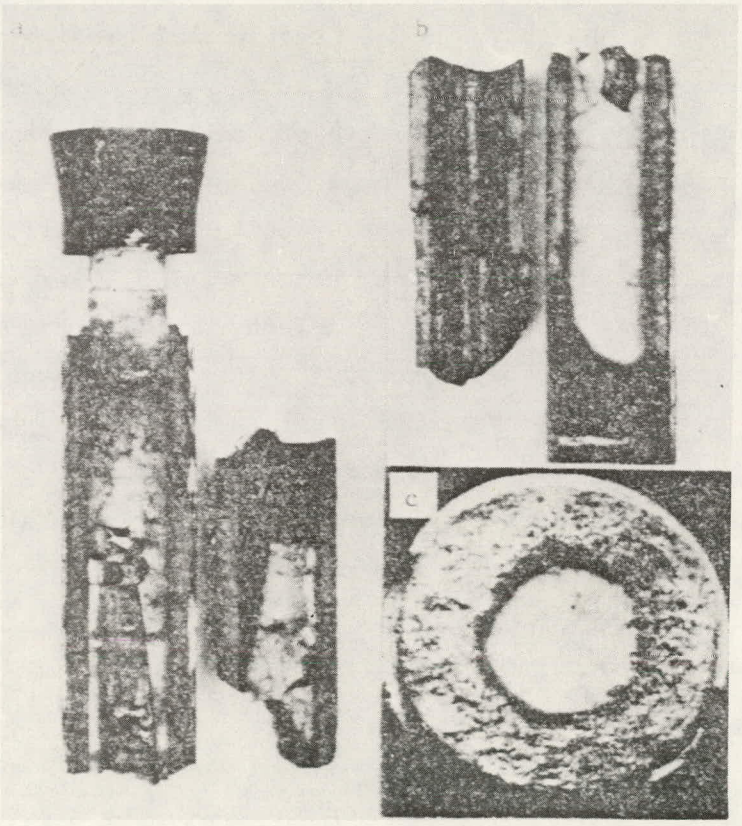

Fig. 5.4 Axial Section of Sulfur Container to Reveal the Condition of the β"-alumina Tube (a) Near the Top, (b) Toward the Bottom of the Cell (Lower Portion of Intact Ceramic Remains Covered with Graphite Felt). End View of Bottom of Tube Appears in (c).

(Figure 5.5), suggests a mixture of phases. Consistent with the radiographic evidence the lower 1.2 cm of the tube was found to be loosely filled with polysulfide similar in appearance to the material at the 8.3 cm level.

(iv) Sulfur electrode (container)

The sodium column was removed with methanol down to a point 4.7 cm below the top edge of the sulfur container, the furthest upward extent of the insurgent polysulfide. Cuts were made through the container wall at distances 2.5, 4.7, 8.3 and 16.5 cm from the top (Figure 5.1) and the container slit axially. The irregularities in the distribution of the graphite felt suggested by the radiographs were confirmed visually.

When the polysulfide-saturated graphite felt was stripped away from the container wall, a thin layer of polysulfide remained attached to the wall and retained numerous graphite fibers from the felt (Figure 5.6a). A piece of the container wall of about 1 cm^2 was sawed from the larger section at a point about 10 cm from the top of the container and boiled in distilled water to remove the polysulfide. During this treatment the graphite fibers became detached from the inside surface. Also a thin, dark, fragile layer conforming to the curvature of the sample became detached from the container wall itself. The inside surface of the detached layer is shown in Figure 5.6b, all the graphite fibers having been detached in the boiling water treatment. This fragile layer appears to be largely graphite flakes from the polyphenylene resin-graphite coating. Energy dispersive X-ray spectroscopy (EDS) of such flakes supports this view. The material that continues to adhere to the container wall is shown in Figure 5.6c and appears to be relatively continuous, although the surface is covered with a network of cracks. The shallow grooves in the background are machining marks on the underlying steel surface.

A micrograph of a transverse section through the container wall and remaining coating is shown in Figure 5.7a. Comparison with the structure of the coating from a section of an unused test container prepared in the same way appears in Figure 5.7b. In the latter instance, the graphite flakes and fibers are the lightest gray constituent, while the polyphenylene resin is somewhat darker. In the sample removed from the cell, on the other

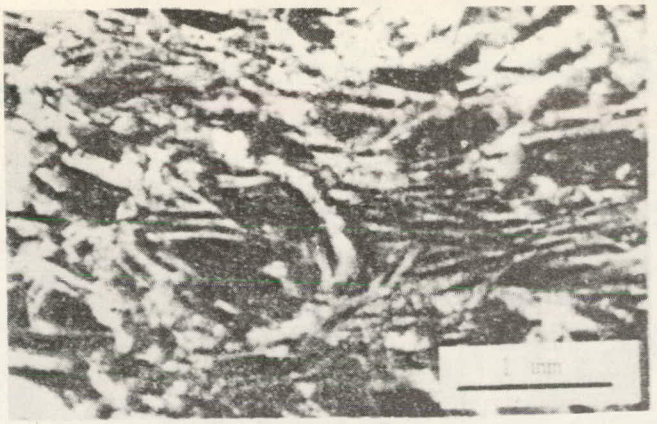

Fig. 5.5 Microstructure of the As-solidified Reactants Found in the β"-alumina Tube at Level 8.3 cm.

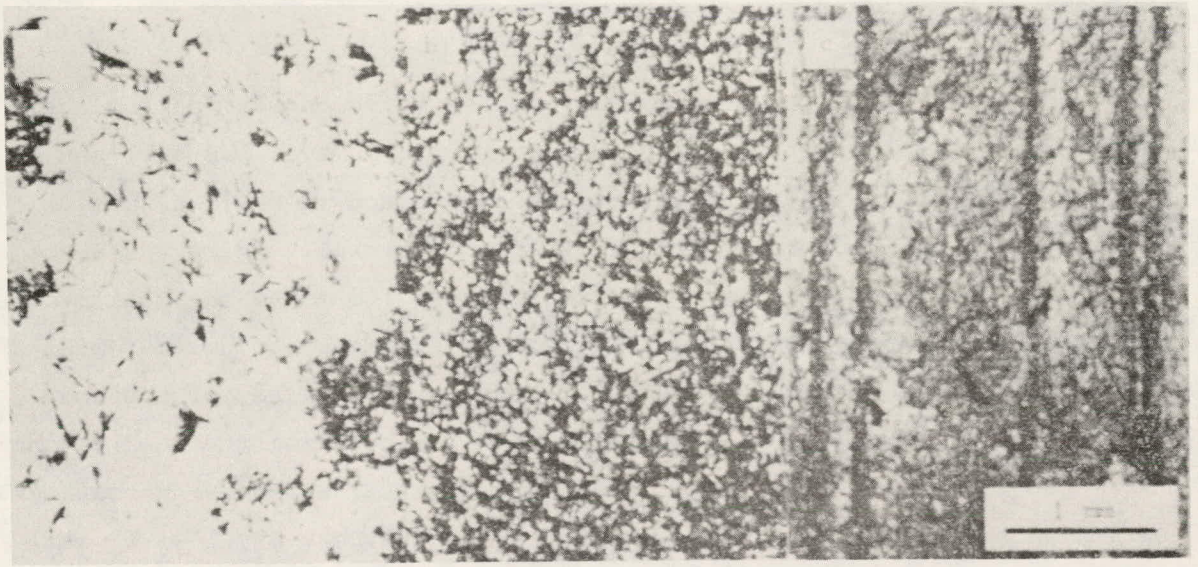

Fig. 5.6 (a) Interior Surface of Polyphenylene Coated Container upon Mechanical Removal of Graphite Felt.
(b) Inside Surface (Wall Facing) of Polyphenylene Layer that Detached During Digestion in Water
(c) Coating Adhering to Container Wall.

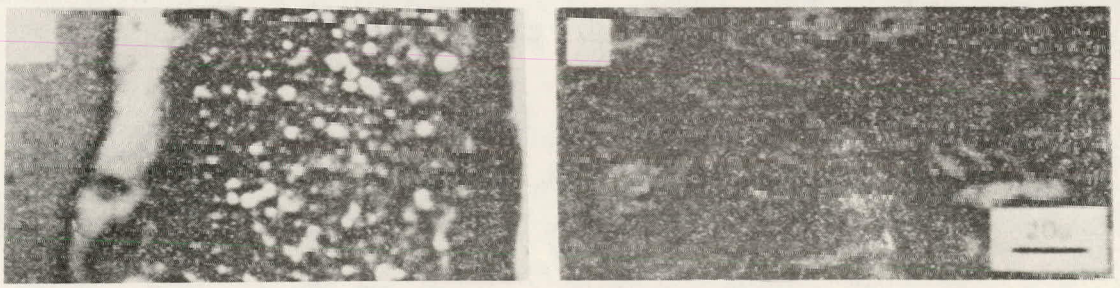

Fig. 5.7 (a) Transverse Section through Container Wall and Remaining Coating
(b) Microstructure of Coating in Initial Condition

hand, the graphite flakes do not appear dominant, the coating apparently being made up of a dark matrix with bright particles embedded in it. A scanning electron micrograph of such a particle and the surrounding matrix appears in Figure 5.8, the accompanying EDS analysis indicating that the particle is principally iron sulfide.

The material at the surface of the coating remaining on the container wall appears in some locations as in the section in Figure 5.9a, while the material adhering to those few spots in which it appeared the coating was absent had a more angular appearance (Figure 5.9b). Both the particle indicated in Figure 5.9a and the overall location in 5.9b contain large amounts of Fe, Cr and S.

The end cap of the cell was left unprotected and upon examination was found to be covered with a dull gray layer. This layer was analyzed by X-ray fluorescence and X-ray diffraction and found to be iron sulfide, FeS_2 (pyrite), plus some other unidentified material. There was also some crystalline material adhering to graphite fibers at the bottom of the cell. The X-ray diffraction pattern of a sample of this material included three lines which matched the unidentified lines of the end cap pattern. Two kinds of crystals were separated from the sample, one dark and one light. On further examination Na, S, and Fe with small amounts of Mn were detected in the dark crystals, and Ti, Al, Si, K with small amounts of Na, Cl, Fe and possibly S were detected in the light colored crystals. It is not unlikely that the end cap served as a source for much of the iron sulfide contamination found in other parts of the cell.

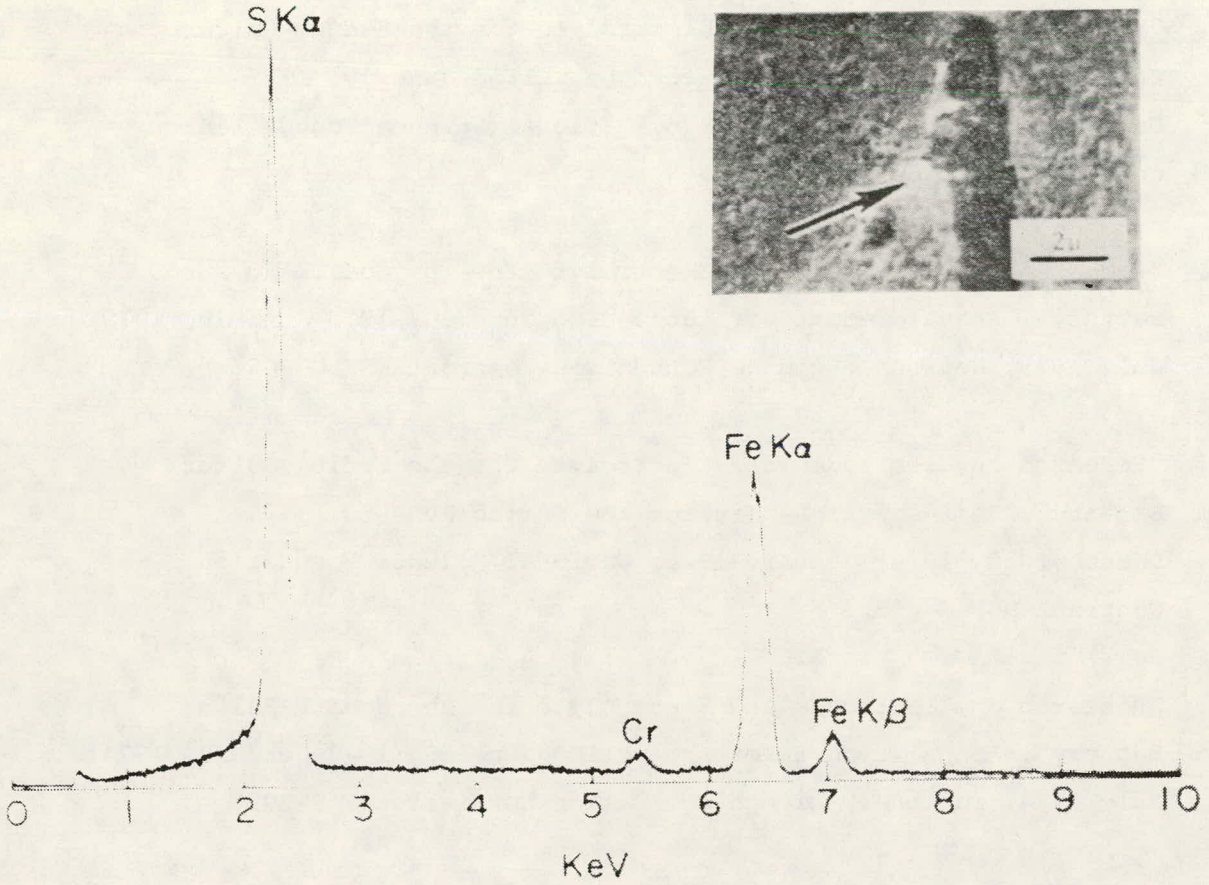

Fig. 5.8 Scanning Electron Micrograph of Matrix and Particle whose X-ray Spectrum is Shown.

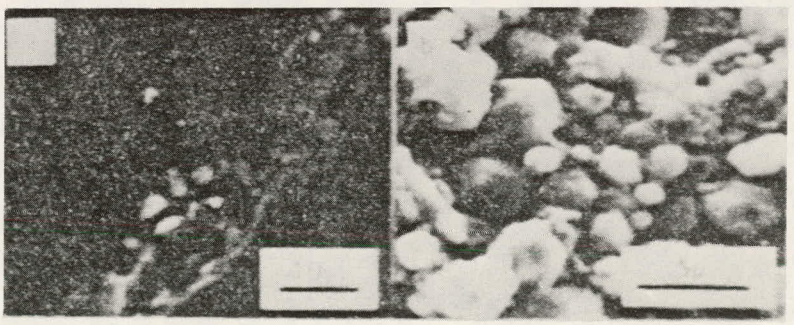

Fig. 5.9 Scanning Electron Micrograph of (a) Residual Coating Remaining at Container Wall (Section) and (b) of Corrosion Product Attached to Metal Wall (Face on)

REFERENCES

1. "Research on Electrodes and Electrolyte for the Sodium-Sulfur Battery", Semi-Annual Report for the period June 30, 1975-December 30, 1975; January 1976, National Science Foundation Contract NSF C-805.

2. "Research on Electrodes and Electrolyte for the Sodium-Sulfur Battery", Annual Report for the period June 30, 1975-June 29, 1975; July 1975, National Science Foundation Contract NSF C-805.

3. "Research on Electrodes and Electrolyte for the Sodium-Sulfur Battery", Semi-Annual Report for the period June 30, 1975-December 30, 1974; January 1975, National Science Foundation Contract NSF C-805.

4. "Research on Electrodes and Electrolyte for the Sodium-Sulfur Battery", Annual Report for the period June 30, 1973-June 29, 1974; July 1974, National Science Foundation Contract NSF C-805.

APPENDIX A

PATENTS

Ford Motor Company

#3,951,689 (5/76), F. A. Ludwig, "Alkali Metal/Sulfur Cell with Gas Fuel Cell Electrode."

#3,966,492 (6/76), F. A. Ludwig, "Sodium Sulfur Battery or Cell with Improved Ampere-Hour Capacity."

#3,976,503 (8/76), R. W. Minck, N. Weber, Y. C. Chang, "Improved Process For Recharging Secondary Batteries"

#3,980, 496 (10/76), F. A. Ludwig, R. W. Minck, S. A. Weiner, "Energy Conversion Devices With Improved Electrode Shapes".

APPENDIX B

PUBLICATION

Ford Motor Company

"The Sodium-Sulfur Battery: A Progress Report," S. A. Weiner, in Energy Storage, pp. 141-154, J. Berkowitz and H. Silverman, ed., Electrochemical Society, Princeton, New Jersey, 1976.

"A Review of the Kinetics of the Sulfur Electrode in Molten Sodium Polysulfide," F. A. Ludwig, Proc. Symp. and Workshop on Advanced Battery Research and Design, March 22-24, 1976, Argonne National Laboratory, ANL-76-0, p. B-117.

"The Performance of Shaped Graphite Electrodes in Sodium-Sulfur Cells." R. W. Minck, Proc. Symp. and Workshop on Advanced Battery Research and Design, March 22-24, 1976, Argonne National Laboratory, ANL-76-8, p. B-199.

"The Sodium-Sulfur Battery: A Progress Report," S. A. Weiner, Proc. Symp. and Workshop on Advanced Battery Research and Design, March 22-24, 1976, Argonne National Laboratory, ANL-76-8, p. B-219.

"The Sulfur Electrode in Non-Aqueous Media," R. P. Tischer and F. A. Ludwig in Advances in Electrochemistry and Electrochemical Engineering, C. W. Tobias and H. Gerischer, ed., Vol. 10.

"Raman Studies of Sulfur-Containing Anions in Inorganic Polysulfides: Barium Trisulfide," G. J. Janz, E. Roduner, J. W. Coutts, and J. R. Downey, Jr., Inorganic Chem. 15, 1751 (1976).

"Raman Studies of Sulfur-Containing Anions in Inorganic Polysulfides: Potassium Polysulfides," C. J. Janz, J. W. Coutts, J. R. Downey, Jr., and E. Roduner, Inorganic Chem. 15, 1751 (1976).

"Raman Studies of Sulfur-Containing Anions in Inorganic Polysulfides: Sodium Polysulfides," C. J. Janz, J. R. Downey, Jr., and E. Roduner, Inorganic Chem. 15, 1759 (1976).

University of Utah

"Crack Front Profiles in Double Torsion Specimens," Anil V. Virkar and Ronald S. Gordon, J. Amer. Ceram. Soc. 58 (11012) 536-537 (1975).

"Application of Load-Relaxation Techniques to Study Subcritical Crack Growth in Brittle Materials," Anil V. Virkar and Ronald S. Gordon, J. Amer. Ceram. Soc. 59 (1-2) 68-71 (1976).

☆U.S. GOVERNMENT PRINTING OFFICE: 1979-640-092/545